International Journal of Modern Physics B
Vol. 23, Nos. 28 & 29 (2009) 5403–5416

CONTINUUM CLIMATE VARIABILITY: LONG-TERM MEMORY, SCALING, AND 1/F-NOISE

KLAUS FRAEDRICH
Meteorological Institute, University of Hamburg, Grindelberg 5,
D-20144 Hamburg, Germany
Klaus.Fraedrich@zmaw.de

RICHARD BLENDER
Meteorological Institute, University of Hamburg, Grindelberg 5,
D-20144 Hamburg, Germany
Richard.Blender@zmaw.de

XIUHUA ZHU
Max-Planck Institute for Meteorology, Bundesstrasse 55,
D-20146 Hamburg, Germany
Xiuhua.Zhu@zmaw.de

Received 21 October 2009

Continuum temperature variability represents the response of the Earth's climate to deterministic external forcing. Scaling regimes are observed which range from hours to millennia with low frequency fluctuations characterizing long-term memory. The presence of $1/f$ power spectra in weather and climate is noteworthy: (i) In the tropical atmosphere $1/f$ scaling ranging from hours to weeks is found for several variables; it emerges as superposition of uncorrelated pulses with individual $1/f$ spectra. (ii) The daily discharge of the Yangtze shows $1/f$ within one week to one year, although the precipitation spectrum is white. (iii) Beyond one year mid-latitude sea surface temperatures reveal $1/f$ scaling in large parts of the global ocean. The spectra can be simulated by complex atmosphere-ocean general circulation models and understood as a two layer heat diffusion process forced by an uncorrelated stochastic atmospheric. Long-term memory on time scales up to millennia are the global sea surface temperatures and the Greenland ice core records (GISP2, GRIP) with δ^{18}O temperature proxy data during the Holocene. Complex atmosphere ocean general circulation models reproduce this behavior quantitatively up to millennia without solar variability, interacting land-ice and vegetation components.

Keywords: Climate variability; long-term memory, $1/f$-noise, detrended fluctuation analysis.

1. Introduction

In the mid 1970s, Brownian motion has entered climate research as a paradigm for the Earth's climate fluctuations. Based on Kutzbach and Bryson's[1] observation that, in the Holocene, temperature variance density increases with decreasing

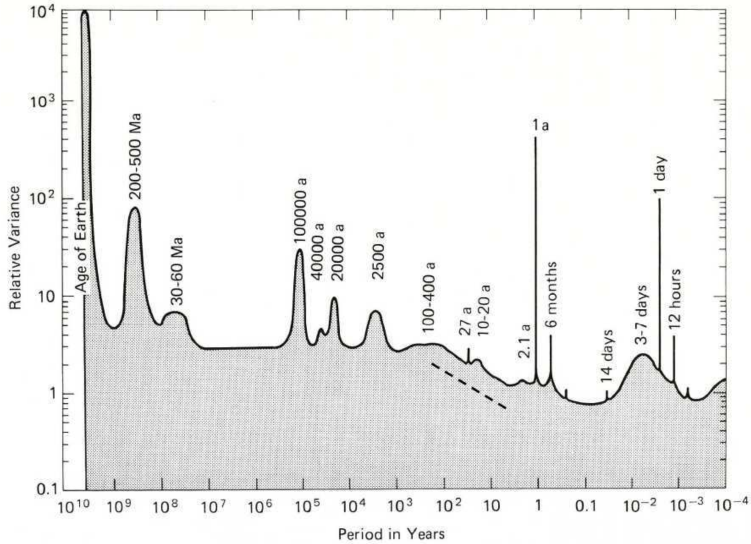

Fig. 1. Sketch of global climate variability (after Ref. 3 and 4). The dashed line indicates long-term memory scaling with $\beta \approx 0.3$ up to centennial time scales.

frequency (Fig. 1), Hasselmann[2] introduced the Brownian motion analog for the climate system response on white noise atmospheric forcing. This Brownian motion paradigm implies a Lorentzian variance spectrum whose density or power spectrum $S(f) \sim f^{-\beta}$ increases with $\beta = 2$ power law and reaches a white noise plateau, $\beta = 0$, at lower frequencies. Although this does not confirm with the Kutzbach and Bryson analysis, such simple concepts have stimulated an intensive red noise search in observed data and simulations of comprehensive coupled atmosphere-ocean general circulation models (AO-GCM).

At the same time, observations and modeling of flicker noise or other power-law scaling regimes emerged[5,6] with concepts as close to the climate system's energy balance as the Brownian analog. Since then power-law power spectra different from Brownian motion have been identified in observed records and model simulations of the climate system. For example, the near surface temperature[7,8] shows low-frequency behavior, which does not, up to very long periods, asymptote towards a white plateau. Huybers and Curry[9] demonstrate that climate variability exists at all timescales with climate processes being intimately coupled; that is, understanding variability at any one timescale requires some understanding of the whole. Here, the power-law relationships of surface temperature variability scale with annual and Milankovitch cycles (23 k and 41 k years, see Fig. 1).

The temporal variability of dynamical systems like weather or climate is conveniently characterized by its memory. Short-term memory shows a finite integral correlation time-scale which is related to exponentially decaying auto-correlation between initial and future states. Long-term memory is characterized by an infinite integral time-scale and has a non-integrable autocorrelation function.[10] Most of the studies are guided by self-affine scaling laws governing the dynamics of a non-linear system,[11] the associated long-range memory or correlation aspect has been considered for observed temperatures[12] and simple GCM simulations.[13] In these studies, the variance spectrum analysis has been determined by detrended fluctuation analysis[14] (DFA). These analyses suggest that the near surface temperature fluctuations are governed by scaling behavior showing long-term memory correlations up to at least thirty years. More recently, links between power law scaling of long-term correlations and the statistics of extremes has been formally established.[15,16,17,18]

A focus of research during the last years was (i) detection of long-term memory in compartments of the global climate system, (ii) its reproducibility by simple and complex models and (iii) its impact on the behavior of trends and extremes. There are three aims underlying this presentation: First, the fluctuation analysis of observed data is extended to all areas where sufficient data has been measured, to detect the geographical distribution of the scaling-law and its dependence on the climate compartment atmosphere, ocean, land and ice (Sec. 2). The second aim addresses the capability of AO-GCMs to reproduce the observed scaling and memory utilizing a 1000 year simulation in a constant greenhouse gas environment. To identify the limit of the memory, scaling of Greenland ice core records (for the Holocene) and temperature fluctuations from ultra-long control simulations of the present day climate are compared (Sec. 2.3). The third aim is to provide a simple explanation for the physics underlying the long-term spectral behavior caused by the complex global oceanic circulation (Sec. 2.4). In Sec. 3 aspects of the long-term memory in the hydrological cycle are considered and Sec. 4 presents a Summary and Conclusion. The observational data sets, climate models, and the detrended fluctuation analysis (DFA) are described in the Appendix.

2. Temperature Variability on Various Time Scales: Air, Land, Ocean, and Ice

Time variability is conveniently represented by a power spectrum. If the spectrum follows a power law scaling for low frequencies, $S(f) \sim f^{-\beta}$, long-term memory can be inferred in the exponent range $0 < \beta < 1$. Flicker or $1/f$-noise[5] ($\beta = 1$) defines the limit for stationarity of stochastic processes; it is associated with intermittency and self-organized criticality. The long-term memory is determined by detrended fluctuation analysis (DFA) which yields $\beta = 2\alpha - 1$ for scaling fluctuation functions, $F(\tau) \sim \tau^{\alpha}$, with the fluctuation exponent α (see Appendix). In this section we review work on the variability on instrumental and simulated surface temperature data in wide ranges of time scales from hours to millennia.

2.1. *Atmospheric variability in the tropics: 1/f-noise and pulses*

Data analysis in the tropical atmosphere shows that, on short time scales, tropical surface conditions may be viewed as alternating between a more quiet or passive phase of a cloud-topped fair weather boundary layer and pulse-like shallow and deep convective events (with drying and cooling of the boundary layer due to downdraughts) embedded in the passive phase. Thus the surface variables need to be analysed in two steps to determine scaling behavior for boundary layer and free atmosphere observables: For the original time series, for time series composed of convective pulses of different duration extracted by wavelets analysis. The data are taken from a 4-month observational period over the tropical Pacific[19] (Tropical Ocean and Global Atmosphere Coupled Ocean-Atmosphere Response Experiment, TOGA-COARE). Power spectra of surface variables reveal a $1/f$-spectrum slope from the 1-hour (minimum period between 0.5 to 5 hours) to the intra-seasonal (30 to 60 day) time scale. This also holds for the free-atmosphere CAPE (Convective Available Potential Energy) which spans the 1–30 day range[20,21] (see also the summarizing Fig. 8).

A concept of continuum $1/f$ variability is gained by a decomposition of the time series into individual pulses. The pulse-like events show no lag-correlation between their recurrence times, that is, individual pulses occur as a Poisson process. This excludes a $1/f$-model, which requires intervals between successive events to be highly correlated. Instead, by lack of correlation, we conclude that the total spectrum (of extracted pulse-like events) can be reproduced by a sum of spectra of individual pulse-like events, which form $1/f$-spectra for ranges exceeding their durations, like cumulus convection with downdraughts, westerly wind bursts of the Madden-Julian (or 30–60 day) oscillation, and possibly ENSO (El Nino-Southern Oscillation).

This scaling behavior poses a challenge to the convective quasi-equilibrium hypothesis, which postulates that cumulus convection responses to large scale forcing in much shorter time than the latter so that convection is almost in equilibrium with the large scale dynamics. If this hypothesis is indeed physically valid, such a short response time must be observationally detectable. This scaling range extends from one hour to beyond ten days for convective and, up to several years, for surface wind stress. This alternative view of convective processes is part of a continuum climate variability extending to longer time scales (decades to millennia) demonstrated in the following subsections by the sea surface temperature (SST) and the ocean circulation variability in the North Atlantic[22] and Greenland ice cores.[23]

2.2. *Decadal atmosphere-ocean variability: Temperature scaling in observations and climate models*

Power-law scaling of near surface air temperature fluctuations and its geographical distribution is analyzed in 100 years instrumental observations and in a 1000 year simulation of the present-day climate with a complex coupled atmosphere-ocean general circulation model[22] (AO-GCM).

First, the observed fluctuation functions are presented at two locations in Central Asia and North Atlantic. The central Asian station [Krasnojarsk, Fig. 2(a)] shows

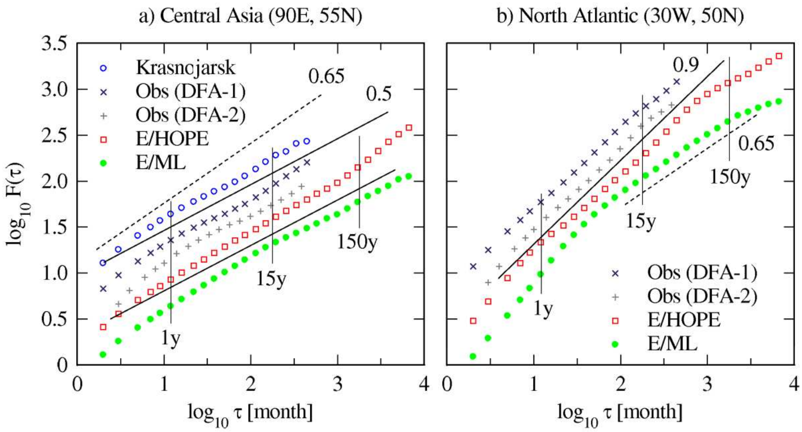

Fig. 2. (Color on line) Temperature fluctuations: in (a) central Asia (90E, 50N) and (b) in the North Atlantic (30W, 50N), calculated for the station Krasnojarsk (93E, 52N), and corresponding regions in the observed grid data set, (Obs), ECHAM4/HOPE and ECHAM4/ML simulations. DFA-1 is used if not indicated otherwise. The exponents are in (a) $\alpha = 0.5$ ($\beta = 0$, solid, white noise), $\alpha = 0.65$ ($\beta = 0.3$, dashed, transition region) and in (b) $\alpha = 0.9$ ($\beta = 0.8$, solid, flicker noise), $\alpha = 0.65$ ($\beta = 0.3$, dashed, transition).

a white power-law ($\alpha = 0.5, \beta = 0$) ranging from one year to decades and the interpolated grid data[24] (CRU) agrees with this in DFA-1 and DFA-2. In the North Atlantic [Fig. 2(b)] the observed grid data shows flicker noise in DFA-1 and DFA-2. The AO-GCM simulation with the complex ocean model (HOPE) reveal a slightly smaller value which, however, extends to longer time scales. The simulation with the simplified mixed layer ocean (ML) shows flicker noise only up to 1–5 years.

The global distribution of temperature fluctuation exponents α (determined by DFA) is derived from the observed monthly near surface temperatures over land and ocean. Inner continental areas in North America and central Asia [Fig. 3(a)] show almost white noise whereas parts of the northern and tropical Atlantic, eastern North-Pacific, and of the Indian Ocean reveal a distinct increase towards flicker noise. Notable is the general tendency of a power law increase from land to sea. In the transition regions, that is, coastal areas and land under maritime influence, the power-law corresponds to $\alpha = 0.65$ ($\beta = 0.3$) found in Ref. 12, as anticipated in the climate variability sketch in Fig. 1.

A 1000 year AO-GCM simulation (ECHAM4/HOPE) in a present-day constant greenhouse gas environment [Fig. 3(b)] agrees closely with the observations. Only in the Indian Ocean and in south-east Asia smaller memory is simulated compared to the observations. The eastern tropical Pacific inhibits power-law scaling within the 1–15 years range due to almost periodic El Nino/Southern Oscillation phenomenon with time scales of 3–7 years. The variability of the power-law exponent α is estimated splitting the 1000 year simulated data in ten non-overlapping 100 year intervals and estimating the exponents in the 1–15 years range. The standard deviation is < 0.05 in most regions.

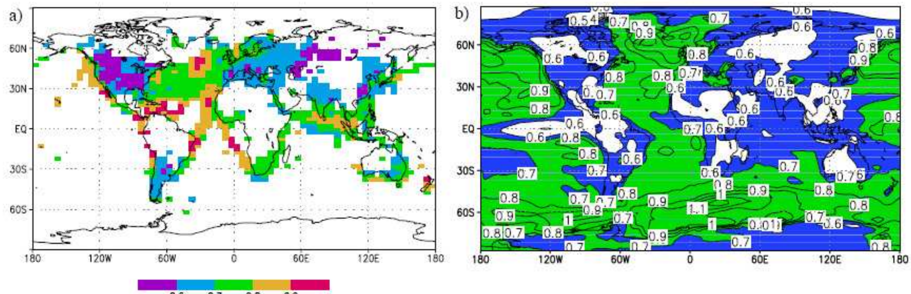

Fig. 3. (Color on line) Fluctuation exponents α: (a) Observed sea surface and near surface air temperatures over land estimated by DFA-2 in 1–15 years. The analysis is restricted to grid points with at least 90% data after 1900. (b) 1000 year coupled atmosphere ocean simulation estimated in 1–15 years (< 0.6 white, 0.6–0.7 blue, > 0.7 green).

On centennial time scales (15 to 150 years) fluctuation exponents are slightly reduced except for the North Pacific, where the $1/f$-spectrum vanishes completely, and for the North Atlantic and the Southern Ocean, where the $1/f$-spectra remain unaffected. The regions of zero memory expand across the tropical belt and the transition areas ($\alpha = 0.6$ to 0.7, $\beta = 0.2$ to 0.4) follow these changes.

Simulations with a mixed layer (ML) model up to 5 years reproduce the main quantitative characteristics of the simulation with a dynamic ocean model (HOPE). However, in 15–150 years, memory in the simulation with the complex ocean fades away approaching white noise. The simulation with prescribed climatological sea surface temperature shows no long-term memory at all. Obviously, the power-law observed in the decadal range can be reproduced by an atmosphere coupled with a ML model, whereas the centennial memory requires a dynamic ocean model.

The spectral variability of the meridional overturning circulation (MOC) in the Atlantic Ocean reveals no consistent result in two coupled AO-GCMs[25] (GFDL and ECHAM5/MPIOM). In the inter-annual to decadal frequency range, the spectra are dominated by scaling, $S(f) \sim f^{-\beta}$, with nontrivial exponents, mostly $\beta \approx 1$, in agreement with $1/f$ or flicker noise. For the lowest frequencies, some spectra show stationary long-term memory, while others reveal spectra increasing with frequency. None of the spectra can be considered uniquely as red noise explained by an ocean integrating a white stochastic atmospheric forcing.

These results show that the simulation with constant atmospheric greenhouse gas concentration reproduces the observed long time memory. Due to the huge temperature increase of the order of 5 K during the next century in a warmer climate it is possible that the long-term memory characteristics change. In two scenario simulations with increasing greenhouse gas concentrations climate models reveal the same global long-term memory structure as in the present-day climate.[26] However, care is needed in the comparison of long-term memory analysis of low resolution gridded model output and station data since slight deviations in the locations may lead to wrong conclusions.

2.3. *Millennial variability: Ice cores and ultra-long AO-GCM simulation*

To identify the limit of the memory, an ultra-long control simulation of a coupled AO-GCM (CSIRO, 10 k years, reduced by a spin-up time) is analyzed and compared with Greenland ice cores (GRIP, GISP2) during the Holocene.[23] The 10,000 year simulation is performed under present-day conditions. Up to 1000 years DFA-scaling leads to a spectral exponent $\beta = 0.5$ in ice-free sea surface temperature south of Greenland consistent with the ice core temperature proxy data. The δ^{18}O ice core records and the sea surface temperatures at nearby model grid points show similar long-term memory up to 1000 years. Beyond that time scale the climate memory appears to fade. It is noteworthy that this long-term memory is simulated without time-dependent external forcings.

The long-term memory (LTM) of the surface temperature is coupled to the intense low frequency variability of the Atlantic MOC (Fig. 4). In the Pacific and the Antarctic Ocean LTM is not simulated, the latter result is in agreement with Antarctic ice core proxy data during the Holocene.

Extending the spectral continuity beyond millennia into the ultra-low frequency domain is one aim of future research, in particular, its conceptual and numerical modeling including continental ice sheet dynamics.

2.4. *Mechanism of $1/f$-noise: Diffusive ocean energy balance model*

The $1/f$-spectrum of the ocean surface temperature in the Atlantic and Pacific mid-latitudes is explained by a vertical diffusion energy balance model consisting of

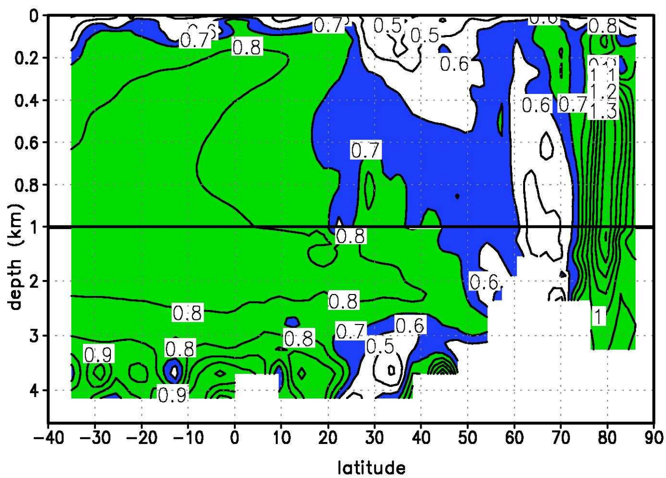

Fig. 4. (Color on line) Fluctuation exponent α of the zonally averaged stream-function (representative for the MOC) in an Atlantic cross section during 100–1000 years (blue: α = 0.6–0.7, β = 0.2–0.4; green: $\alpha > 0.7$, $\beta > 0.4$).

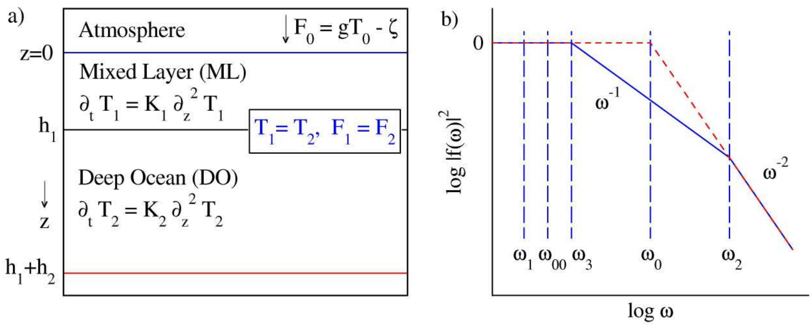

Fig. 5. Two-layer diffusion model: (a) Shallow mixed and deep ocean layer (depths h_1, h_2 and diffusion coefficients K_1, K_2) forced by a heat flux F_0 at the air-sea interface with deterministic (conductivity g) and stochastic contributions. (b) Sketch of response spectra. The (angular) frequency band $\omega_2 > \omega_3$ opens a $1/f$-scaling regime.

a shallow mixed layer on top of a deep ocean forced by stochastic surface fluxes.[27] A 1000 year climate simulation is employed for testing: Given its total surface heat flux forcing at the air-sea interface, the impact of horizontal surface advection and the internal thermal diffusivities can be estimated.

The spectra of the observed and simulated temperature variability of the large ocean basins may be explained by a simple two-layer vertical diffusion model of temperature anomalies in a shallow mixed layer on top of a deep ocean characterized with (not necessarily) different diffusion coefficients [Fig. 5(a)]. Typical values are for the mixed layer and deep ocean depths, $h_1 = 50$ m, $h_2 = 1000$ m, and the respective diffusivities, $K_1 = 10^{-3}\,\mathrm{m}^2\,\mathrm{s}^{-1}$, $K_2 = 10^{-5}\ \mathrm{m}^2\,\mathrm{s}^{-1}$ (Ref. 28). The surface heat flux drives the fluctuations by a linear plus random contribution,[29] $F_0 = gT_0 - \zeta$; conductance $g \sim 10^{-6}\,\mathrm{ms}^{-1}$ and residual noise are determined by regression analysis from the millennium simulation. At the layer-interface temperature and fluxes are continuous; at the bottom, the anomalous heat flux vanishes. The response —R—2 is schematically presented in Fig. 5(b): A $1/f$-regime emerges in the frequency range, $\omega_2 \sim K_2/h_1^2$ and $\omega_3 \sim g^2/K_2$, with larger (smaller) frequencies following a Lorentzian (white) scaling.[6] In this interval, the $1/f$-spectral band opens as a distinct scaling region. Long-term correlations in the mixed layer commence beyond its diffusive time scale, h_1^2/K_1, when it is fully affected by the deep ocean diffusive flux with time scale h_1^2/K_2. They decay at time scales beyond K_2/g_2, when a mixed layer temperature change due to the surface heat flux exceeds deep ocean diffusive flux. The other frequencies are $\omega_0 \sim g/h_1$, $\omega_{00} \sim g/(h_1 + h_2)$, $\omega_1 \sim K_2/h_2^2$. Representative comparison with measurements is obscured by the relatively short observational period, so that a millennium simulation is used to provide a consistent data set, which yields the surface conductance g by regression, the power spectra of the mean mixed layer temperature S and of the residual heat flux S^*. This leads to a consistent verification of the mixed layer response $|R|^2 = g^2 S/S^*$, which is demonstrated for regions in the ocean basins. This concept is in line with the issue that the general circulation of the oceans and its meridional overturning is linked with small scale mixing processes, instead of being a heat engine.[30]

3. The Hydrological Cycle: Rain, Rivers, and Moisture

The long-term memory of the surface temperature and runoff is outstanding since other prominent key variables like pressure and precipitation[31] indicate much less memory. Long-term memory analysis of the components of the hydrological cycle in East Asia in a high resolution GCM simulation reveals specific differences between the variables that describe processes (precipitation, evaporation, and local runoff) and those describing storage[32] (soil wetness, soil temperature, and, similar, atmospheric near-surface temperature). The simulated river flows of the Yangtze reveal LTM with scaling exponents $\beta = 0.3 \cdots 0.4$ extending beyond the decadal time scale (similar to observations, and that of the rivers Nile and Huang He.[33]

3.1. *Yangtze runoff, floods, and droughts*

The Yangtze Delta is located in Eastern China and characterized by the subtropical monsoon climate. The mean annual precipitation is 1235 mm with summer rainfall (June-August) accounting for 40% of the total and only 11% occur during winter months (December-February). This area is densely populated and climate variability is documented for more than 1000 years.

The daily Yangtze discharge variability reveals distinct $1/f$ variability within the weekly to the annual timescale.[34] The origin of this variability in the upper, mountainous reaches of the catchment is not known since precipitation is uncorrelated in this area. The extreme variability leads to severe ecological stresses and, on the other hand, hampers discharge forecasts. In the lower reaches the high frequency variability is reduced, probably due to river-lake exchange and subsurface flows.

The hydrological conditions in the Yangtze delta are characterized by floods and droughts. In our analysis[33] we use historical documents to derive decadal time series of flood and drought occurrence in the middle Yangtze and the Yangtze Delta for the period 1000 to 1950 [Fig. 6(a)]. The long-term memory in these time series is determined by DFA and reveals scaling power-spectra with a spectral exponent $\beta \approx 0.3$ up to centennial time scales [Fig. 6(b)].

The long-term memory of reconstructed floods and droughts agrees with the long-term memory in discharge measurements and runoff simulations in an AO-GCM simulation (300 years present-day control run).[32]

3.2. *Extreme event return times in high resolution mixing ratio data with $1/f$ spectrum*

The distribution of extreme event return times and their correlations are analyzed in observed and simulated long-term memory[16,17] (LTM) time series with $1/f$ power spectra.[18] The analysis is based on tropical temperature and mixing ratio (specific

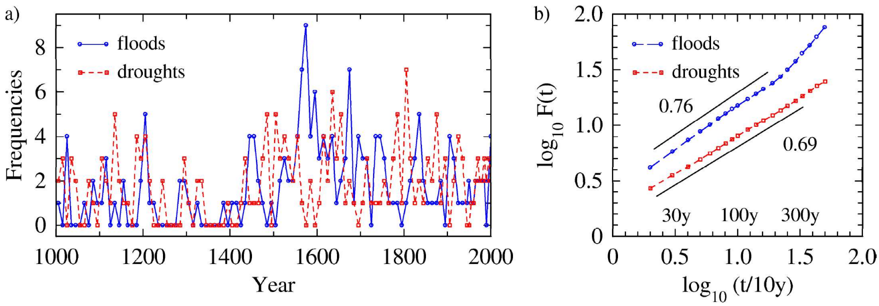

Fig. 6. (a) Floods and droughts in the Yangtze Delta reconstructed by historical documents (number of events per decade). (b) Fluctuation functions obtained by DFA of floods and droughts; slopes indicate long-term memory power-law exponents α in the fluctuation function.

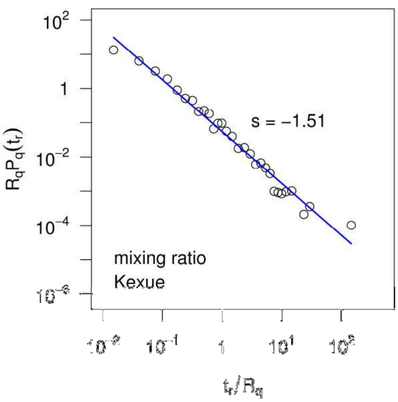

Fig. 7. Return time distribution for the observed mixing ratio (Kexue) for the mean return time $R_q = 100$. The blue curve is a power law fit with slope $s = -1.51$.

humidity) time series from TOGA COARE[19] with 1 min resolution and an approximate $1/f$ power spectrum. Extreme events are determined by Peak-Over-Threshold (POT) crossing. The Weibull distribution represents a reasonable fit to the return time distributions. The mixing ratio measured at research vessel (R/V) Kexue has sufficiently many time steps ($\approx 10^5$) to allow an extreme event analysis. The return time distribution $P_q(t_r)$ for the mixing ratio is determined using the mean return time $R_q = 100$. The distribution in Fig. 7 can be represented by a power law with the slope $s = -1.51$ in a wide range of the ratios r/R_q.

For a comparison and an analysis of the return time predictability, a very long simulated time series with an approximate $1/f$ spectrum is produced by a fractionally differenced (FD) process.[35] This simulated data confirms the Weibull distribution (a power law can be excluded). The return time sequences show distinctly weaker long-term correlations than the original time series (correlation exponent $\gamma \approx 0.56$).

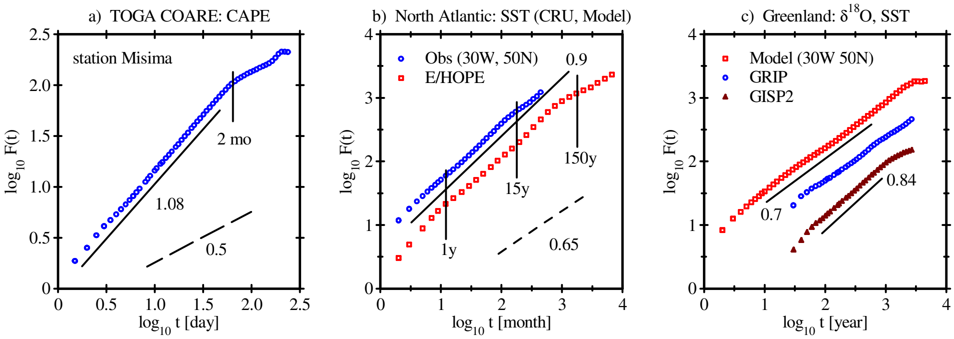

Fig. 8. Climate variability in (a) tropical data (CAPE, TOGA-COARE) in the short-term range of days to months, (b) mid-latitude sea surface temperature (SST) in the North Atlantic in the annual to decadal time range (observed and simulated) , and (c) in Greenland ice core and simulated SST in the decadal to millennial time range. The panels show the DFA fluctuation functions; its power law scaling is marked by slopes α corresponding to spectral power law scaling $\beta = 2\alpha - 1$.

4. Summary and Conclusion

In summarizing, these analyses demonstrate that the variability of the near surface temperature shows a continuum of long-term memory which can be modeled by complex state-of-the-art climate models. The spectral behavior of global fields of observed and simulated surface temperatures is analyzed using detrended fluctuation analysis. Some of the main results for the scaling of the climate variability are combined in Fig. 8:

- In the atmosphere, the high frequency range is assessed by observations in the tropical western Pacific [Fig. 8(a)]. Here Convective Available Potential Energy (CAPE) shows a $1/f$ spectrum (obtained by DFA) within 1 to 30 days,[20] while temperature, wind speed, and moisture show this spectrum within 1 hour to 10 days. Modeling of variability on shortest time scales is still unsatisfactory, for example, tropical convective processes in the time domain of hours to weeks and, not independently, river discharges on daily time scales. In these applications subscale processes are involved, which need to be parameterized even in high resolution climate models.
- The observed sea surface temperature in the North Atlantic shows a $1/f$ spectrum on intra-annual time scales[22] [Fig. 8(b)]. AO-GCM simulations predict centennial $1/f$ variability also in extended regions also in the Southern Ocean. In the inner continents, memory is absent (white noise). In coastal regions and areas under maritime influence a transition between white and flicker noise is observed. The scaling variability is estimated by ten 100 year intervals of the simulation, lies within 0.025–0.05. According to the simulation, the power-law extends up to 15–150 years. Since this correlation is found only if the atmosphere is coupled to the complex ocean model, the origin of the memory can be traced back to the internal long time memory of ocean dynamics.

- Greenland ice cores present a proxy for temperature variability revealing scaling long-term memory on millennial time scales which is simulated by an ultra-long AO-GCM simulation[23] [Fig. 8(c)]. It is remarkable that the AO-GCM CSIRO used in this study is neither forced externally nor coupled to interacting vegetation and land-ice components.

Conceptual diagnostics and models have been developed for the high frequency tropical boundary layer variability and for the low frequency sea surface temperature $1/f$ scaling:

- For the tropical atmospheric variability a conceptual approach is based on random pulses affecting a boundary layer recharge-discharge mechanism.[20] The surprising outcome of this reasoning is that individual pulses are not correlated. The overall $1/f$ spectrum is generated by individual pulses given by $1/f$-noise in a range exceeding the duration of the pulses' life-time.
- The $1/f$ variability in parts of the global ocean[22] (North Atlantic and the Southern Ocean) can be modeled by stochastically forced two-layer heat diffusion.[27] The main results are (i) the theoretical model requires two layers with extremely different diffusivities, representing a mixed layer on top of an deep abyssal ocean, (ii) the atmospheric forcing needs to be white, and (iii) the model predicts ranges of the diffusivity of the deep ocean, which is extremely hard to measure.

Acknowledgments

We like to thank the German Science Foundation (DFG, SFB 512/D1) and the Klima Campus Hamburg.

Appendix A. Data, Models, and Analysis

Data: In the analyses we use three main data sets: (i) The observed global near surface temperature data is a combination of near surface air temperatures over land and sea surface temperatures (SST) interpolated to a $5° \times 5°$-grid (CRU, Climate Research Unit, East Anglia.[24] Monthly data is available since 1856, however, the predominance of missing values in the global data set limits the correlation analysis to a belt from North America to Europe (including the North Atlantic), India and south-east Asia, and small areas in the southern hemisphere. We restrict the application of the DFA to those grid points with less than 10% missing data after 1900. (ii) The central Asian station data at Krasnojarsk (93E, 52N; 1915–1999) is compared with the corresponding grid data. (iii) High frequency variability is analyzed in data measured during the Tropical Ocean and Global Atmosphere Coupled Ocean-Atmosphere Response Experiment[19] (TOGA COARE, November 1992 — February 1993) at the research vessel Kexue with 1 min resolution (specific humidity).

Models: The simulations are based on several atmosphere ocean general circulation models (AO-GCMs), all simulations are present-day control-runs: (i) A 1000 years simulation with ECHAM4/HOPE.[36] ECHAM4 has a horizontal resolution of $3.75° \times 3.75°$ and 19 vertical levels. The ocean is simulated by the comprehensive dynamic model HOPE (resolution $2.8° \times 2.8°$ and 20 vertical levels including sea ice dynamics. The mixed layer (ML) model is restricted to the uppermost ocean layer. (ii) A 350 years control run with the updated version ECHAM5 coupled to MPIOM (formerly HOPE). (iii) The 10,000 years simulation with the model CSIRO Mark 2 (horizontal resolution $5.2° \times 3.2°$) which includes a dynamic ocean and thermodynamic sea ice model; land ice and vegetation are fixed.[23] (iv) The Planet Simulator (University of Hamburg) is an Ocean-Atmosphere General Circulation Model built to perform numerical experiments for understanding the dynamics of the climates of the Earth, Earth-like planets, and moons of the solar system.[37] (v) A 500 years simulation with the GFDL model[38] version CM2.1 ($2° \times 2°$ resolution and 24 levels) coupled to an ocean model ($1° \times 1°$ resolution and 50 vertical levels).

Analysis: The long-term correlations are deduced by the detrended fluctuation analysis (DFA).[14] The DFA determines time scale dependent fluctuations in stationary anomaly sequences with long time correlation. First, the anomaly time series is integrated to the so-called profile. In time segments of length τ, the fluctuation F(?) of the profile with respect to linear fits in each segment is determined and then averaged over all segments. Polynomial trends of order $N-1$ in the time series are eliminated by the DFA-N, which subtracts polynomial fits of order N from the profile in each segment (linear trends will be subtracted by DFA-2). For power-laws in the correlation function, $C(\tau) \sim \tau^{-\gamma}$, the fluctuation function is $F(\tau) \sim \tau^{\alpha}$ and the power (or variance) spectrum is $S(f) \sim f^{-\beta}$ with $\beta = 2\alpha - 1$ and $\alpha = 1 - \gamma/2$. The power-law exponents for stationary processes with long-term memory are between white noise ($\alpha = 0.5, \beta = 0$) and flicker or $1/f$-noise ($\alpha = \beta = 1$).

References

1. J. E. Kutzbach and R. A. Bryson, *J. Atmos. Sci.* **31**, 1958 (1974).
2. K. Hasselmann, *Tellus* **28**, 473 (1976).
3. J. M. Mitchell, *Quatern. Res.* **6**, 481 (1976).
4. M. Ghil and S. Childress, *Topics in Geophysical Fluid Dynamics: Atmospheric Dynamics, Dynamo Theory, and Climate Dynamics* (Springer-Verlag, New York, 1987).
5. R. F. Voss and J. Clarke, *Phys. Rev. B* **13**, 556 (1976).
6. K. M. van Vliet, A. van der Ziel and R. R. Schmidt, *J. Appl. Phys.* **51**, 2947 (1980).
7. S. Manabe and R. J. Stouffer, *J. Climate* **9**, 376 (1996).
8. J. D. Pelletier, *J. Climate* **10**, 1331 (1997).
9. P. Huybers and W. Curry, *Nature* **441**, 329 (2006).
10. J. Beran, *Statistics for Long-Memory Processes* (Chapman & Hall, New York, 1994).
11. J. D. Pelletier and D. Turcotte, *Adv. Geophys.* **40**, 91 (1999).
12. E. Koscielny-Bunde, A. Bunde, S. Havlin, H. E. Roman, Y. Goldreich and H.-J. Schellnhuber, *Phys. Rev. Lett.* **81**, 729 (1998).
13. W. Müller, R. Blender and K. Fraedrich, *Nonlin. Proc. Geophys.* **9**, 37 (2002).
14. C.-K. Peng, S. V. Buldyrev, S. Havlin, M. Simons, H. E. Stanley and A. L. Goldberger, *Phys. Rev. E* **49**, 1685 (1994).

15. T. Antal, M. Droz, G. Györgyi and Z. Rácz, *Phys. Rev. Lett.* **87**, 240601 (2001).
16. E. G. Altmann and H. Kantz, *Phys. Rev. E* **71**, 056106 (2005).
17. J. F. Eichner, J. W. Kantelhardt, A. Bunde and S. Havlin, *Phys. Rev. E* **75**, 011128 (2007).
18. R. Blender, K. Fraedrich, and F. Sienz, *Nonlin. Proc. Geophys.* **15**, 557 (2008).
19. P. Webster and R. Lukas, *Bull. Amer. Meteor. Soc.* **73**, 1377 (1992).
20. J.-I. Yano, K. Fraedrich and R. Blender, *J. Climate* **14**, 3608 (2001).
21. J.-I. Yano, R. Blender, C. Zhang and K. Fraedrich, *Quart. J. R. Meteorol. Soc.* **130**, 1697 (2004).
22. K. Fraedrich and R. Blender, *Phys. Rev. Lett.* **90**, 108501 (2003).
23. R. Blender, K. Fraedrich and B. Hunt, *Geophys. Res. Lett.* **33**, L04710 (2006).
24. D. E. Parker, C. K. Folland and M. Jackson, *Climatic Change* **31**, 559 (1995).
25. X. Zhu, K. Fraedrich and R. Blender, *Geophys. Res. Lett.* **33**, L21603 (2006).
26. R. Blender and K. Fraedrich, *Geophys. Res. Lett.* **30**(14), 1769 (2003).
27. K. Fraedrich, U. Luksch and R. Blender, *Phys. Rev. E* **70**, 037301 (2004).
28. W. Munk and C. Wunsch, *Deep-Sea Research I*, **45**, 1977 (1998).
29. R. L. Haney, *J. Phys. Oceanography* **1**, 241 (1971).
30. C. Wunsch and R. Ferrari, *Annu. Rev. Fluid. Mech.* **36**, 281 (2004).
31. K. Fraedrich and C. Larnder, *Tellus* **45A**, 289 (1993).
32. R. Blender and K. Fraedrich, *Int. J. Climatol.* **26**, 1547 (2006).
33. T. Jiang, Q. Zhang, R. Blender and K. Fraedrich, *Theor. Appl. Clim.* **82**, 131 (2005).
34. G. Wang, T. Jiang, R. Blender and K. Fraedrich, *J. Hydrology* **351**, 230 (2008).
35. J. R. M. Hosking, *Biometrika* **68**, 165 (1981).
36. E. Roeckner *et al.*, Report No. 218, Max-Planck-Institute for Meteorology, Hamburg, 1996.
37. K. Fraedrich, H. Jansen, E. Kirk, U. Luksch and F. Lunkeit, *Meteorol. Zeitschrift* **14**, 299 (2005).
38. T. L. Delworth, A. J. Broccoli, A. Rosati, R. J. Stouffer, V. Balaji, J. A. Beesley, W. F. Cooke, K. W. Dixon, J. Dunne and K. A. Dunne, *J. Clim.* **19**, 643 (2006).